Theoretical studies of bound configuration levels and their radiative lifetimes in Pd^- and Pt^-

C. X. Song,[1] S. J. Wu,[1] K. Wang,[2] X. M. Zhang,[1] R. Si,[1,*] and C. Y. Chen[1,†]

[1]*Shanghai EBIT Lab, Key Laboratory of Nuclear Physics and Ion-beam Application, Institute of Modern Physics, Department of Nuclear Science and Technology, Fudan University, Shanghai 200433, China*

[2]*Department of Physics and Anhui Key Laboratory of Optoelectric Materials Science and Technology, Key Laboratory of Functional Molecular Solids, Ministry of Education, Anhui Normal University, Wuhu, Anhui 241000, China*

(Received 20 June 2022; accepted 28 November 2022; published 22 December 2022)

We performed multiconfiguration Dirac-Hartree-Fock and relativistic configuration-interaction calculations for states of the $4d^9 5s^2$ and $4d^{10}5s$ configurations in Pd^- and for states of the $5d^9 6s^2$ and $5d^{10}6s$ configurations in Pt^-. Valence-valence, core-valence, and core-core electron correlation effects are accounted for in the present studies. The calculated excited energy levels agree within 2.5% with the available experimental values for both Pd^- and Pt^- and we confirm that Pd^- only has one bound excited state. We report a more precise value for the radiative lifetime of $5d^9 6s^2\ ^2D_{3/2}$ in Pt^- (67.0 ± 0.3 ms), which agrees within the experimental range (50–200 ms), but the radiative lifetime of $5d^{10}6s\ ^2S_{1/2}$ (4.00 ± 0.16 s) in Pt^- is 50% longer than the experimental measurement (2.54 ± 0.10 s). The radiative lifetimes for $4d^9 5s^2\ ^2D_{3/2,5/2}$ in Pd^- are also discussed in detail.

DOI: 10.1103/PhysRevA.106.062820

I. INTRODUCTION

The study of negative ions has been an area of considerable interest over the past few decades and plays important roles in many branches of physics and chemistry [1–3]. Due to the lack of long-range Coulomb potential, negative ions usually can only form a few bound states and generally only one ground state. For negative ions with more than one bound state, most of the excited states have the same configuration as the ground state. According to the selection rule of transitions, their radiative lifetimes are dominated by E1 forbidden transitions, such as M1 or E2 transitions. Until now, only four anions have been confirmed to exist as bound states with opposite parities, namely, La^-, Os^-, Ce^-, and Th^- [4–9], and our recent work shows Th^- as an excellent candidate for laser cooling of negative ions [9,10].

For different reasons, negative ions pose a challenge to both theorists and experimentalists. Since electron correlation effect is more enhanced in negative ions than in the isoelectronic atoms and positive ions, the accurate description of electron correlation is highly demanding in theoretical studies. Experimentally, due to the fragility of negative ions, the production in sufficient quantities and the storage over long times are both difficult tasks.

The cases we study here are Pt^- and Pd^-; both of them have more than one bound state and, in particular, the bound states are in two different electronic configurations, albeit in the same parity. The ground states of neutral Pd and Pt are $4d^{10}$ and $5d^9 6s$, respectively. Both of the anions can form bound states in $nd^{10}(n+1)s$ and $nd^9(n+1)s^2$ ($n =$ 4 and 5 for Pt^- and Pd^-, respectively), but the ground state of Pd^- lies in $4d^{10}5s\ ^2S_{1/2}$, while for Pt^- it lies in $5d^9 6s^2\ ^2D_{5/2}$. Previous experiments have observed one bound excited state $4d^9 5s^2\ ^2D_{5/2}$ of Pd^- [11,12], the former performed by Feigerle *et al.* using laser photoelectron spectroscopy yielded the excitation energy 1097(65) cm^{-1} [11] and the latter performed by Scheer *et al.* using laser photodetachment threshold spectroscopy gave 1127(4) cm^{-1} [12], but whether $4d^9 5s^2\ ^2D_{3/2}$ is weakly bound or slightly unbound with respect to the ground state remains inconclusive. For Pt^-, the excitation energy of $5d^9 6s^2\ ^2D_{3/2}$ was measured to be 9740.9(5) cm^{-1} by Thøgersen *et al.* via two-photon detachment spectroscopy [13], Andersson *et al.* determined the second excitation energy of $5d^{10}6s\ ^2S_{1/2}$ to be 10289(13) cm^{-1} using laser photodetachment threshold spectroscopy [14].

Recently, Chartkunchand *et al.* [15] has first reported the radiative lifetimes of the $5d^{10}6s\ ^2S_{1/2}$ and $5d^9 6s^2\ ^2D_{3/2}$ bound excited states in Pt^- measured at the Double ElectroStatic Ion Ring Experiment (DESIREE) facility. However, only a lifetime in the range of 50–200 ms could be estimated for $5d^9 6s^2\ ^2D_{3/2}$ [15]; the accuracy needs to be improved by theoretical studies. The lifetime of $5d^{10}6s\ ^2S_{1/2}$ state was measured to be 2.54 ± 0.10 s [15], but there were no theoretical results to compare with; a first theoretical study is very essential. From the theoretical point of view, the radiative lifetimes of $^2D_{3/2}$ and $^2S_{1/2}$ are dominated by two different types of transition rates, M1 and E2 transitions, respectively. The M1 line strength is independent of the radial part of the wave function in pure *LS* approximation and the transition rate can be obtained analytically by the aid of an experimental wavelength; whether this approximation is still suitable for heavy systems needs to be verified by *ab initio* relativistic calculations. The E2 transition rate is a challenge for theoretical study, especially when between two different configurations;

*rsi@fudan.edu.cn
†chychen@fudan.edu.cn

here we studied how the electron correlation affects the transition wavelength and line strength, which could serve as a reference for future theoretical studies. For Pd^-, no experimental measured lifetime has been reported until now, which also asks for theoretical studies.

In this paper, applying the multiconfiguration Dirac-Hartree-Fock (MCDHF) and relativistic configuration-interaction (RCI) method [16], we present theoretical studies on the energy levels and radiative lifetimes of the states in $nd^{10}(n+1)s$ and $nd^9(n+1)s^2$ configurations of Pd^- and Pt^-. The theoretical results are compared with the experimental values.

II. THEORETICAL APPROACH

A. MCDHF

The relativistic MCDHF method, implemented in the GRASP code [17,18], is employed in the present paper. The starting point for our fully relativistic calculations is the Dirac-Coulomb Hamiltonian

$$H_{\rm DC} = \sum_{i=1}^{N}[c\,\boldsymbol{\alpha_i}\cdot\boldsymbol{p_i} + (\beta_i - 1)c^2 + V_i] + \sum_{i<j}^{N}\frac{1}{r_{ij}}, \quad (1)$$

where V_i is the central part of the electron-nucleus Coulomb interaction, $\boldsymbol{\alpha}$ and β are the 4×4 Dirac matrices, and c is the speed of light in atomic units. In the MCDHF method, the atomic state wave function (ASF) $\Psi(\gamma PJ)$ of parity P, the total angular momentum J, can be expanded over the configuration state functions (CSFs) with the same parameter

$$\Psi(\gamma PJ) = \sum_{i=1}^{N} c_i\Phi(\gamma_i PJ), \quad (2)$$

where γ is the orbital occupancy and angular coupling tree quantum numbers. The CSFs are the summation of the antisymmetrical product of the single-electron Dirac wave functions

$$\phi_{n\kappa m} = \frac{1}{r}\begin{pmatrix} P_{n\kappa}(r)\chi_{\kappa m}(\theta,\phi) \\ iQ_{n\kappa}(r)\chi_{-\kappa m}(\theta,\phi)\end{pmatrix}, \quad (3)$$

where $P_{n\kappa}(r)$ and $Q_{n\kappa}(r)$ represent the large and small components of the radial wave function, respectively.

In this work, the wave functions were determined in the extended optimal level (EOL) scheme [19] and the radial parts of the Dirac orbitals and the expansion coefficients were obtained iteratively in the relativistic self-consistent field (RSCF) scheme. The transverse interaction in the low-frequency limit, or the Breit interaction

$$H_{\rm Breit} = -\sum_{j>i}^{N}\frac{1}{2r_{ij}}\left[(\boldsymbol{\alpha_i}\cdot\boldsymbol{\alpha_j}) + \frac{(\boldsymbol{\alpha_i}\cdot\boldsymbol{r_{ij}})(\boldsymbol{\alpha_j}\cdot\boldsymbol{r_{ij}})}{r_{ij}^2}\right], \quad (4)$$

and leading QED (vacuum polarization and self-energy) were included in subsequent relativistic configuration-interaction (RCI) calculations, where now only the expansion coefficients were determined by diagonalizing the Hamiltonian matrix. To calculate the spin-angular part of the matrix elements, the second quantization method in coupled tensorial form and quasispin technique [20] was adopted.

B. Transition parameters

Transition parameters, such as transition rates and line strengths between two states $\Psi(\gamma PJ)$ and $\Psi(\gamma' P'J')$, are expressed in terms of reduced matrix elements of the relevant transition operators [21]:

$$\langle\Psi(\gamma PJ)||\mathbf{T}||\Psi(\gamma' P'J')\rangle = \sum_{k,l} c_k c_l'\langle\Phi(\gamma_k PJ)||\mathbf{T}||\Phi(\gamma_l' P'J')\rangle. \quad (5)$$

The line strength (S, in a.u.) is related with the transition rate (A, in s^{-1}) by the standard equations given below. For the M1 transition

$$A_{ji}^{\rm M1} = \frac{2.6974\times 10^{13}}{\omega_j\lambda_{ji}^3}S^{\rm M1}, \quad (6)$$

for the E2 transition

$$A_{ji}^{\rm E2} = \frac{1.1199\times 10^{18}}{\omega_j\lambda_{ji}^5}S^{\rm E2}, \quad (7)$$

where λ_{ji} is the transition energy or wavelength in Å, and ω_i and ω_j are the statistical weights of the lower (i) and upper (j) levels.

Other than the *ab initio* calculated results, we can adjust the radiative rate with the experimental energy according to

$$A_{\rm M1,adjusted} = \left(\frac{\lambda_{ab\,initio}}{\lambda_{\rm expt}}\right)^3 A_{{\rm M1},ab\,initio}, \quad (8)$$

for M1 transitions, and

$$A_{\rm E2,adjusted} = \left(\frac{\lambda_{ab\,initio}}{\lambda_{\rm expt}}\right)^5 A_{{\rm E2},ab\,initio}, \quad (9)$$

for E2 transitions, which can eliminate the uncertainty caused by the calculated wavelengths.

III. CALCULATIONS AND RESULTS

A. Computation strategy

We first performed Dirac-Hartree-Fock (DHF) calculations for the three states ($^2S_{1/2}$ and $^2D_{3/2,5/2}$) associated with the $nd^9(n+1)s^2$ and $nd^{10}(n+1)s$ configurations in Pd^- and Pt^-. These orbitals are kept fixed in the following calculations. The CSF expansions are obtained using the restricted active set (RAS) method, by allowing single and double (SD) substitutions from the "single" reference (SR) configurations, $nd^9(n+1)s^2$ and $nd^{10}(n+1)s$, to the active set space [22]. We define the outermost nd and $(n+1)s$ electrons as valence electrons and the remaining as core electrons. When the substitutions are all from valence electrons, VV (valence-valence) correlation is included; CV (core-valence) correlation is included when we also allow at the most a single substitution from the core subshells; CC (core-core) correlation can be included when we allow both single and double substitutions from the core subshells. In the present paper, for example, VV means that only VV correlation is included; CV_{4d} means that VV correlation, CV/CC correlations of the inner subshells than $4d$ and CV correlation of $4d$ are included; CC_{4d} means CC correlation of the $4d$ subshell is also included. The active set space is increased up to $n\leqslant 10, l\leqslant 6$ (AS_{10}) layer by layer, where the active set is labeled by its maximum principle

TABLE I. Configurations from which the CSFs contribute more than 0.1% to the wave-function compositions

Config.	$\sum c_i^2$	Config.	$\sum c_i^2$
Pd^- $4d^{10}5s$ $^2S_{1/2}$		Pt^- $5d^{10}6s$ $^2S_{1/2}$	
$4d^{10}5s$	90.7	$5d^{10}6s$	89.4
$4d^84f^25s$	1.7	$5d^85f^26s$	1.5
Pd^- $4d^95s^2$ $^2D_{3/2}$		Pt^- $5d^96s^2$ $^2D_{3/2}$	
$4d^95s^2$	91.4	$5d^96s^2$	90.2
$4d^74f^25s^2$	0.2	$5d^96p^2$	0.4
$4d^95p^2$	0.1	$5d^75f^26s^2$	0.1
Pd^- $4d^95s^2$ $^2D_{5/2}$		Pt^- $5d^96s^2$ $^2D_{5/2}$	
$4d^95s^2$	91.5	$5d^{10}6s$	89.4
$4d^74f^25s^2$	0.3	$5d^96p^2$	0.3
$4d^95p^2$	0.1	$5d^75f^26s^2$	0.1

quantum number. In the RSCF procedure, only VV correlation was included; CV and CC correlations due to the core electrons down to $3s$ (for Pd^-) and $4s$ (for Pt^-) subshells were taken into account by restricted substitutions step by step to show their importance in the RCI procedure.

Since negative ions are strong-correlated systems, SD substitutions from the SR configurations are normally not enough to capture all the correlation effects; triple and quadruple (TQ) substitutions are also of great importance [23,24]. By analyzing the wave-function compositions from the SR calculations, we extract a set of multireference (MR) configurations from which the sum of the wave-function compositions is larger than 0.1%, as shown in Table I, and allow SD substitutions from these configurations; in this way we can include the important TQ substitutions from the SR configurations and, more importantly, get a balance of level energies from different configurations.

B. Energy levels

The relative energy levels (transition energies) between $^2S_{1/2}$ and $^2D_{3/2,5/2}$ in Pd^- and Pt^- from different correlation models are shown in Fig. 1 and listed in Tables II and III. We can see that the fine-structure splitting between $^2D_{3/2}$ and $^2D_{5/2}$ is relatively stable with respect to the CV and CC correlation effects; the relative discrepancies between different correlation models are generally within 2%. However, the relative position of the $^2D_{3/2,5/2}$ levels and the $^2S_{1/2}$ level is quite sensitive to the core correlation effects; for example, the excitation energy of $^2S_{1/2}$ relative to $^2D_{3/2}$ in Pt^- from the CC_{5p} model is twice as large as that from the VV model; there even exists a level crossing between $^2S_{1/2}$ and $^2D_{5/2}$ in Pd^-, which makes the ground state of Pd^- flip between these two levels. With the opening of core subshells down to $3s$ (for Pd^-) and $4s$ (for Pt^-), we can see that the relative positions of the three levels reached excellent convergence, which illustrates that we have included enough core correlations.

As mentioned earlier, further SD substitutions from MR configurations are essential to balance the level energies from different configurations. By investigating the wave-function compositions from the above calculations, we noticed that

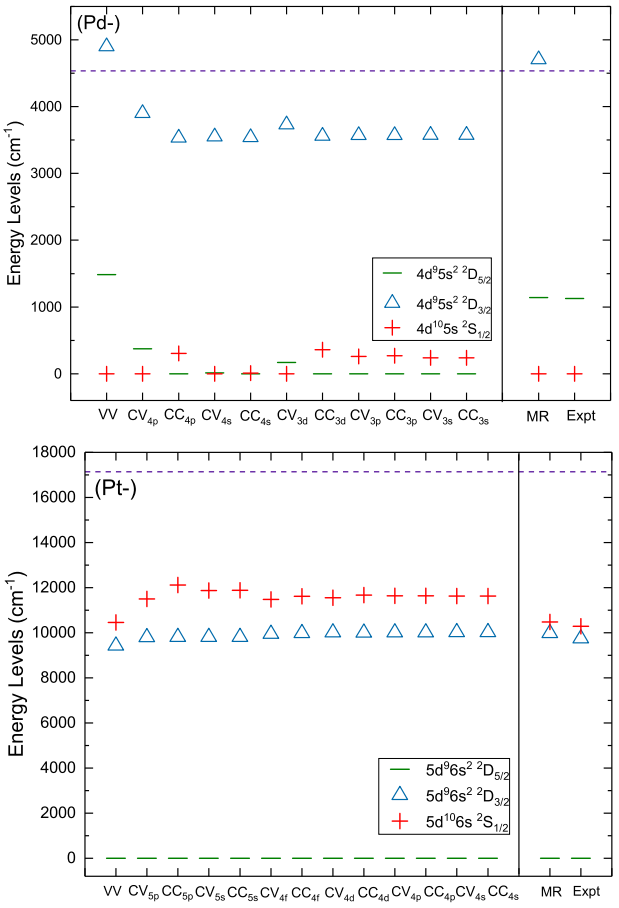

FIG. 1. Calculated energy levels from different correlation models of the SR calculations. The final results from the MR calculations and experimental measurements [12–14] are also shown. The horizontal lines represent the experimental electron affinities of Pd and Pt [12,26].

TABLE II. Present *ab initio* transition energies (ΔE, in cm^{-1}), line strengths (S, in a.u.), and transition rates (A, in s^{-1}) for Pd^- from different calculation models. $a[b] \equiv a \times 10^b$.

	$^2D_{5/2} - {}^2S_{1/2}$			$^2D_{3/2} - {}^2D_{5/2}$		
	ΔE	S	A	ΔE	S	A
DHF	−10360	19.98	1.33[−01]	3537	2.3982	0.7155
SR calculations						
VV	1486	23.34	3.16[−06]	3413	2.3982	0.6431
CV_{4p}	374	22.41	3.07[−09]	3527	2.3986	0.7098
CC_{4p}	−304	22.35	3.25[−09]	3531	2.3985	0.7123
CV_{4s}	−12	22.11	9.79[−17]	3537	2.3985	0.7160
CC_{4s}	10	22.11	1.16[−16]	3538	2.3985	0.7164
CV_{3d}	171	21.75	5.88[−11]	3560	2.3985	0.7297
CC_{3d}	−360	21.28	7.16[−09]	3560	2.3985	0.7297
CV_{3p}	−259	21.23	1.37[−09]	3570	2.3985	0.7359
CC_{3p}	−269	21.19	1.67[−09]	3572	2.3985	0.7369
CV_{3s}	−240	21.18	9.44[−10]	3574	2.3985	0.7386
CC_{3s}	−240	21.17	9.43[−10]	3574	2.3985	0.7386
MR calculations						
	1141	21.49	7.77[−07]	3564	2.3984	0.7323

TABLE III. Present *ab initio* transition energies (ΔE, in cm^{-1}), line strengths (S, in a.u.), and transition rates (A, in s^{-1}) for Pt^- from different calculation models.

	$^2S_{1/2} - {}^2D_{5/2}$			$^2D_{3/2} - {}^2D_{5/2}$		
	ΔE	S	A	ΔE	S	A
DHF	19796	37.98	6.465	9444	2.3874	13.559
SR calculations						
VV	10460	41.12	0.288	9422	2.3902	13.483
CV_{5p}	11501	39.98	0.450	9795	2.3940	15.171
CC_{5p}	12111	40.01	0.584	9802	2.3937	15.204
CV_{5s}	11874	39.76	0.525	9811	2.3938	15.242
CC_{5s}	11887	39.75	0.528	9810	2.3938	15.240
CV_{4f}	11480	38.92	0.435	9951	2.3937	15.903
CC_{4f}	11620	38.53	0.457	9975	2.3933	16.020
CV_{4d}	11556	38.44	0.444	10010	2.3932	16.188
CC_{4d}	11670	38.42	0.466	10002	2.3931	16.145
CV_{4p}	11638	38.39	0.459	10012	2.3930	16.195
CC_{4p}	11635	38.38	0.458	10014	2.3930	16.203
CV_{4s}	11625	38.38	0.456	10016	2.3930	16.214
CC_{4s}	11624	38.38	0.456	10016	2.3930	16.215
MR calculations						
	10483	38.69	0.274	9980	2.3931	16.039

CSFs arising from the $nd^9(n+1)p^2$, $nd^8nf^2(n+1)s$, and $nd^7nf^2(n+1)s^2$ configurations also have non-negligible contributions to the wave-function compositions, as shown in Table I, which is caused by the strong interaction between $nd^2 \leftrightarrow nf^2$ and $ns^2 \leftrightarrow np^2$. These configurations are defined as the MR set; CSFs generated by SD substitutions from their valence electrons to $8s8p8d7f6g$ and $9s9p9d8f7g$ for Pd^- and Pt^- are also included in our final calculations. The final MR calculations consist of 587 729, 1 408 103, and 1 994 691 CSFs distributed on the $J = 1/2, 3/2, 5/2$ symmetries for Pd^- and 644 972, 1 597 456, and 2 342 446 CSFs on the $J = 1/2, 3/2, 5/2$ symmetries for Pt^-. Hence we not only included the important TQ substitutions from $nd^9(n+1)s^2$ and $nd^{10}(n+1)s$ configurations, but also obtained a balance between the energy levels generated from them.

The comparisons of MR results with the experimental and other theoretical values are shown in Table IV. For the two bound excitation states of Pt^- ($^2D_{3/2}$ and $^2S_{1/2}$) and the single measured excitation state of Pd^- ($^2D_{5/2}$), the calculated excitation energies (9980 cm^{-1}, 10483 cm^{-1}, and 1141 cm^{-1}) agree with the experimental values (9740.9 cm^{-1}, 10289 cm^{-1}, and 1127 cm^{-1}) [12–14] by within 2.5%. Comparing with the previous MCDF calculation [13] performed using the GRASP92 program [25], from which the bound excited energies for Pt^- are 9535 cm^{-1} and 11301 cm^{-1}, respectively, the present calculation gives a better agreement with the measurement for the latter level. For the second excited state of Pd^- ($^2D_{3/2}$), our calculation gives 4706 cm^{-1}, which is 172 cm^{-1} higher than the measured electron affinity of Pd, 4534.0(10) cm^{-1} [12]. As shown in Table II, the fine-structure splitting of $^2D_{3/2,5/2}$ is quite stable with respect to electron correlations; the estimated uncertainty of our calculated $^2D_{3/2,5/2}$ splitting is within 15 cm^{-1}. On the other hand, the excitation level of $^2D_{5/2}$ is only 14 cm^{-1} higher than the experimental measurement; we estimate the uncertainty of our calculated $^2D_{3/2}$ level in Pd^- is within 30 cm^{-1}, which means that this level is an unbound state.

C. Line strengths and radiative lifetimes

In Fig. 2, we show our calculated line strengths between $^2D_{5/2}$ and $^2S_{1/2}$ levels for Pd^- and Pt^- from different correlation models of the SR calculations; the E2 transition between these two levels dominates the radiative lifetime of the upper one. For $^2D_{3/2}$ levels in both Pd^- and Pt^-, their radiative lifetimes are dominated by the M1 transition to $^2D_{5/2}$; the calculated line strengths similar to Fig. 2 are shown in Fig. 3. The line strengths as well as the transition rates are also listed in Tables II and III. By considering the *ab initio* and adjusted M1 and E2 transition rates [see Eqs. (6)–(9)] between these levels, the *ab initio* and adjusted lifetimes for the excitation states are listed in Table IV.

The uncertainties of the calculated lifetime (transition rate) generally come from two aspects—transition wavelength and line strength. From Figs. 2 and 3 and Tables II and III, we can see that the line strengths are well converged with respect to electron correlations. Comparing with the values from the VV calculations, CV/CC correlation effects reduced the E2 line

TABLE IV. *Ab initio* transition energies (ΔE, in cm^{-1}), line strengths (S, in a.u.), transition rates (A, in s^{-1}), and radiative lifetimes (τ, in s) from the present MR calculations. The previous MCDF calculation results, experimental values, adjusted transition rates, and radiative lifetimes by using the experimental transition wavelengths are also shown. Estimated uncertainties are given in parentheses. $a[b] \equiv a \times 10^b$.

		Present *ab initio*				Other theo. [13]		Expt. [12–14]		Adjusted	
Upper	Lower	ΔE	S	A	τ	ΔE	τ	ΔE	τ	A	τ
Pd^-											
$^2D_{5/2}$	$^2S_{1/2}$	1141	21.5	7.77[−7]	1.29(13)[+6]			1127(4)		7.29[−7]	1.37(7)[+6]
$^2D_{3/2}$	$^2D_{5/2}$	3564	2.40	7.32[−1]	1.36						
$^2D_{3/2}$	$^2S_{1/2}$	4706	12.6	8.16[−4]							
Pt^-											
$^2D_{3/2}$	$^2D_{5/2}$	9980	2.39	1.60[+1]	0.0623(50)	9535	0.071	9740.9(5)	0.05–0.2	14.9	0.0670(3)
$^2S_{1/2}$	$^2D_{5/2}$	10483	38.7	2.74[−1]	3.65(48)	11301		10289(13)	2.54(10)	0.250	4.00(16)
$^2S_{1/2}$	$^2D_{3/2}$	504	17.9	3.25[−8]							

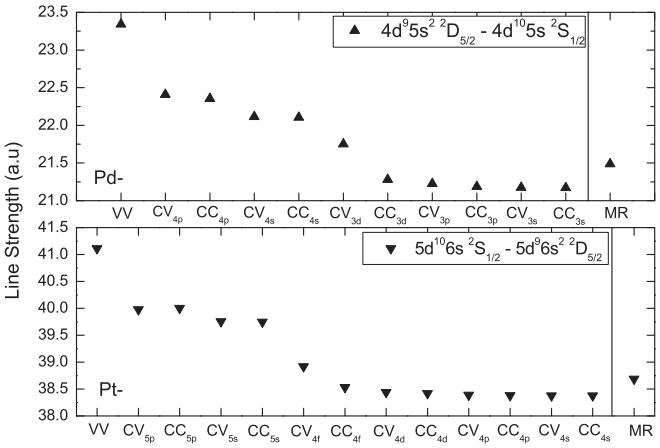

FIG. 2. Calculated E2 line strengths from different correlation models of the SR calculations and the final results from the MR calculations.

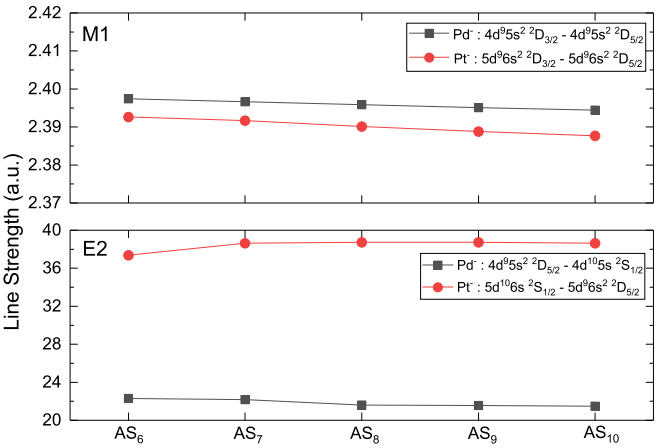

FIG. 4. Calculated line strengths as a function of maximum principal quantum number of the active sets.

strengths for Pd^- and Pt^- by 10% and 7%, respectively. On the other hand, the M1 line strengths are more stable; CV/CC correlation effects only raised the VV results for Pd^- and Pt^- by 0.01% and 0.1%, respectively. Opening more inner core subshells will generate a tremendous number of CSFs and is beyond our calculation ability; here we take the contribution of $CC/CV_{4d,4p,4s}$ correlations as our calculation uncertainty due to the closed $n \leqslant 3$ shells for Pt^- and the contribution of $CC/CV_{3p,3s}$ correlations as the uncertainty due to the closed $n \leqslant 2$ shells for Pd^-; they are 0.5% and 0.01% for the E2 and M1 transitions. When expanding the SR configuration to MR configurations, the E2 line strengths for Pd^- and Pt^- increased by 1.5% and 0.8%, respectively, while the M1 line strengths barely changed; we take this difference as the uncertainty arising from missed high-order substitutions. In Fig. 4, we show the final calculated line strengths as a function of the active sets, from which we estimate the uncertainties due to limited n values of the active space for E2 and M1 transitions are 0.6% and 0.1%, respectively. We can see that the line strengths are quite stable from different perspectives; by summing the above possible uncertainties together, the uncertainties from line strengths to the E2 and M1 transition rates are 3% and 0.2%, respectively.

By comparing with the experimental observations, we get that the uncertainties from transition wavelengths to the $^2S_{1/2} \rightarrow {}^2D_{5/2}$ and $^2D_{3/2} \rightarrow {}^2D_{5/2}$ transition rates in Pt^- are 10% and 8%, respectively; after rescaling the transition rate using the observed wavelength and taking into account the experimental error, the uncertainties can be eliminated by a large extent to 0.7% and 0.2%, respectively. The uncertainties from transition wavelengths before and after rescaling to the $^2D_{5/2} \rightarrow {}^2S_{1/2}$ transition rate in Pd^- are 7% and 2%, respectively.

Adding the uncertainties coming from line strengths and transition wavelengths together, the estimated uncertainties for our *ab initio* calculated radiative lifetimes of $^2S_{1/2}$ and $^2D_{3/2}$ in Pt^- are 13% and 8%, respectively; the adjusted uncertainties are 4% and 0.4%, respectively. The uncertainties for the *ab initio* calculated and adjusted radiative lifetimes of $^2D_{5/2}$ in Pd^- are 10% and 5%, respectively. The estimated errors are also listed in Table IV. For $^2D_{3/2}$ in Pd^-, since we have no experimental excitation energy to compare with, we only listed its *ab initio* calculated radiative lifetime. It should be noted that since it is an unbound sate, decays via autodetachment will shorten its lifetime further and beyond the scope of the present paper [11].

From Table IV, we can see that for $^2D_{3/2}$ in Pt^-, both our *ab initio* calculated (62.3 ms) and the adjusted (67.0 ms) lifetimes using the experimental transition wavelengths fall within the estimated experimental range (50–200 ms) [15], and agree well with the previous MCDF calculation (71 ms) [13] and analytical result (66.9 ms) [27]. For $^2S_{1/2}$ in Pt^-, neither the *ab initio* calculated (3.65 s) nor the adjusted (4.00 s) values agree within the experimental error bar (2.54 ± 0.10 s) [15]. Although we cannot give an exact explanation for the disagreement, this is not surprising because the long-lived excited states in anions easily detach electrons when colliding with residual gas present in a particle trap or along a beam line [28], which makes the measurement very difficult and sometimes underestimates the radiative lifetime. For example, the radiative lifetime for the excited $3d^94s^2\ {}^2D_{3/2}$ in Ni^- was measured to be 15.1 ± 0.4 s [29], but is 25% shorter

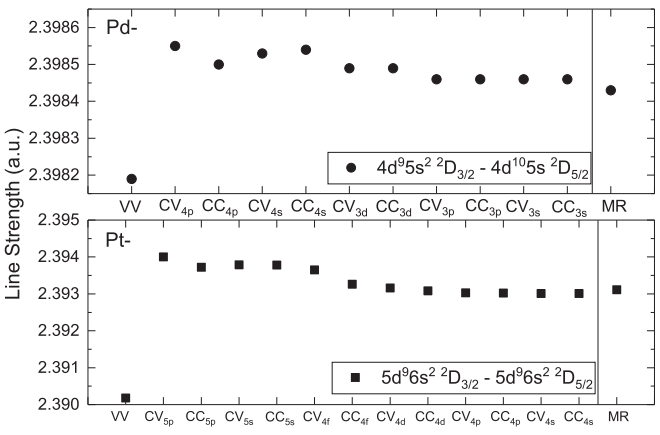

FIG. 3. Same as Fig. 2, but for M1 transitions.

than the elaborate calculation (18.86 s) [30]. For Pd^-, the radiative lifetime for $^2D_{5/2}$ is around 15 days, which means this is a typical metastable state and its lifetime is very hard to measure.

IV. CONCLUSION

Applying the MCDHF and RCI method, we performed theoretical studies on the bound configuration states in Pd^- and Pt^-. Our study shows the importance of core correlation and high-order substitutions to balance the energy levels from different configurations. The agreement between our calculated excitation energy levels and the available experimental values is within 2.5%, and our calculation shows that $4d^9 5s^2\ ^2D_{3/2}$ in Pd^- is an unbound state, which was inconclusive in previous studies.

In contrast to energy levels, the calculated line strength is quite stable with respect to different calculation models, by taking into account the possible uncertainties arising from the inactive core subshells, limited n values of the active set space, and higher-order substitutions and, with the aid of the experimental transition wavelengths, we give a more precise radiative lifetime for $5d^9 6s^2\ ^2D_{3/2}$ in Pt^- (67.0 ± 0.3 ms) than the experimental measurement (50–200 ms), but for $5d^{10}6s\ ^2S_{1/2}$, the present theoretical value (4.00 ± 0.16 s) is 50% longer than the experimental value (2.54 ± 0.10 s), which requires further study.

ACKNOWLEDGMENTS

This work is supported by the National Natural Science Foundation of China (Grants No. 12104095, No. 12074081, and No. 12074082). K.W. acknowledges the support from the Natural Science Foundation of Hebei Province, China (Grant No. A2019201300).

[1] S. Petrie, Mon. Not. R. Astron. Soc. **281**, 137 (1996).
[2] L. K. Fifield, Rep. Prog. Phys. **62**, 1223 (1999).
[3] J. C. Rienstra-Kiracofe, G. S. Tschumper, H. F. Schaefer, S. Nandi, and G. B. Ellison, Chem. Rev. **102**, 231 (2002).
[4] C. W. Walter, N. D. Gibson, Y.-G. Li, D. J. Matyas, R. M. Alton, S. E. Lou, R. L. Field, D. Hanstorp, L. Pan, and D. R. Beck, Phys. Rev. A **84**, 032514 (2011).
[5] R. C. Bilodeau and H. K. Haugen, Phys. Rev. Lett. **85**, 534 (2000).
[6] U. Warring, M. Amoretti, C. Canali, A. Fischer, R. Heyne, J. O. Meier, C. Morhard, and A. Kellerbauer, Phys. Rev. Lett. **102**, 043001 (2009).
[7] C. W. Walter, N. D. Gibson, D. J. Matyas, C. Crocker, K. A. Dungan, B. R. Matola, and J. Rohlén, Phys. Rev. Lett. **113**, 063001 (2014).
[8] E. Jordan, G. Cerchiari, S. Fritzsche, and A. Kellerbauer, Phys. Rev. Lett. **115**, 113001 (2015).
[9] R. Tang, R. Si, Z. Fei, X. Fu, Y. Lu, T. Brage, H. Liu, C. Chen, and C. Ning, Phys. Rev. Lett. **123**, 203002 (2019).
[10] R. Tang, R. Si, Z. Fei, X. Fu, Y. Lu, T. Brage, H. Liu, C. Chen, and C. Ning, Phys. Rev. A **103**, 042817 (2021).
[11] C. S. Feigerle, R. R. Corderman, S. V. Bobashev, and W. C. Lineberger, J. Chem. Phys. **74**, 1580 (1981).
[12] M. Scheer, C. A. Brodie, R. C. Bilodeau, and H. K. Haugen, Phys. Rev. A **58**, 2051 (1998).
[13] J. Thøgersen, M. Scheer, L. D. Steele, H. K. Haugen, and W. P. Wijesundera, Phys. Rev. Lett. **76**, 2870 (1996).
[14] P. Andersson, A. O. Lindahl, D. Hanstorp, and D. J. Pegg, Phys. Rev. A **79**, 022502 (2009).
[15] K. C. Chartkunchand, M. Kaminska, E. K. Anderson, M. K. Kristiansson, G. Eklund, O. M. Hole, R. F. Nascimento, M. Blom, M. Bjorkhage, A. Kallberg *et al.*, Phys. Rev. A **94**, 032501 (2016).
[16] C. F. Fischer, M. Godefroid, T. Brage, P. Jönsson, and G. Gaigalas, J. Phys. B **49**, 182004 (2016).
[17] P. Jönsson, G. Gaigalas, J. Bieroń, C. Froese Fischer, and I. P. Grant, Comput. Phys. Commun. **184**, 2197 (2013).
[18] C. Froese Fischer, G. Gaigalas, P. Jönsson, and J. Bieroń, Comput. Phys. Commun. **237**, 184 (2019).
[19] K. Dyall, I. Grant, C. Johnson, F. Parpia, and E. Plummer, Comput. Phys. Commun. **55**, 425 (1989).
[20] G. Gaigalas, Z. Rudzikas, and C. Froese Fischer, J. Phys. B: At., Mol., Opt. Phys. **30**, 3747 (1997).
[21] R. D. Cowan, *The Theory of Atomic Structure Spectra* (University of California Press, Berkeley, CA, 1981).
[22] J. Olsen, B. O. Roos, P. Jørgensen, and H. J. A. Jensen, J. Chem. Phys. **89**, 2185 (1988).
[23] R. Si and C. F. Fischer, Phys. Rev. A **98**, 052504 (2018).
[24] R. Si, S. Schiffmann, K. Wang, C. Y. Chen, and M. Godefroid, Phys. Rev. A **104**, 012802 (2021).
[25] F. Parpia, C. Fischer, and I. Grant, Comput. Phys. Commun. **94**, 249 (1996).
[26] R. C. Bilodeau, M. Scheer, H. K. Haugen, and R. L. Brooks, Phys. Rev. A **61**, 012505 (1999).
[27] T. Brage and J. Grumer, J. Phys. B: At., Mol., Opt. Phys. **50**, 025001 (2017).
[28] H. T. Schmidt *et al.*, Rev. Sci. Instrum. **84**, 055115 (2013).
[29] M. Kaminska, V. T. Davis, O. M. Hole, R. F. Nascimento, K. C. Chartkunchand, M. Blom, M. Bjorkhage, A. Kallberg, P. Lofgren, P. Reinhed *et al.*, Phys. Rev. A **93**, 012512 (2016).
[30] R. Si, C. Y. Zhang, K. Yao, T. Brage, C. Y. Chen, and Y. M. Zou, Phys. Rev. A **95**, 042504 (2017).